Journal of Alzheimer's Disease 80 (2021) 775–786
DOI 10.3233/JAD-201419
IOS Press

Evaluation of Fluorinated Cromolyn Derivatives as Potential Therapeutics for Alzheimer's Disease

Timothy M. Shoup[a], Ana Griciuc[b], Marc D. Normandin[a], Luisa Quinti[b], Lindsay V. Walsh[b], Maeva Dhaynaut[a], Sung-Hyun Moon[a], Nicolas J. Guehl[a], Pedro Brugarolas[a], David R. Elmaleh[a,c,*], Georges El Fakhri[a,*] and Rudolph E. Tanzi[b]
[a]*Gordon Center for Medical Imaging, Massachusetts General Hospital, Boston, MA, USA*
[b]*Genetics and Aging Research Unit, McCance Center for Brain Health, Mass General Institute for Neurodegenerative Disease, Department of Neurology, Massachusetts General Hospital and Harvard Medical School, Charlestown, MA, USA*
[c]*AZTHERAPIES, INC., Boston, MA, USA*

Accepted 6 January 2020
Pre-press 12 February 2021

Abstract.
Background: Cromolyn is an anti-neuroinflammatory modulator with a multifactorial mechanism of action that has been shown to inhibit amyloid-β (Aβ) aggregation and enhance microglial uptake and clearance of Aβ.
Objective: We report the effects of fluoro-cromolyn derivatives on microglial cell toxicity and microglial clearance of $A\beta_{42}$.
Methods: Microglial cell toxicity for cromolyn derivatives were determined in naive BV2 microglial cells. Microglial clearance assays were performed with $A\beta_{42}$ in naive BV2 microglial cell line and single cell clone BV2 line expressing $CD33^{WT}$. PET imaging was performed for three F-18 analogs in a rhesus macaque.
Results: All compounds but derivative **8** exhibited low microglial cell toxicity. Cromolyn **1** and derivatives **2**, **4**, and **7** displayed an increased uptake on $A\beta_{42}$ in naïve BV2 microglial cells. Derivative **4** increased $A\beta_{42}$ uptake in a dose-dependent manner and at 75 μM resulted in a one-fold increase in $A\beta_{42}$ uptake in BV2-$CD33^{WT}$. PET imaging for three [^{18}F]cromolyn analogs revealed the order of brain tracer penetration to be **4a** > **10** > **2a**. Tracer **4a** exhibited enhanced uptake in areas of high perfusion (putamen, grey matter, and cerebellum) and lower signal in areas of lower perfusion (caudate, thalamus, and white matter).
Conclusion: Substantial uptake of $A\beta_{42}$ in both naïve BV2 and BV2-$CD33^{WT}$ cells observed with **4** indicate conversion of microglial cells from a pro-inflammatory to an activation state favoring Aβ phagocytosis/clearance. These findings suggest that a fluoro-cromolyn analog could reduce fibril-prone $A\beta_{42}$ *in vivo* and thereby serve as a therapeutic for the treatment and prevention of AD.

Keywords: Aβ phagocytosis, Alzheimer's disease therapy, amyloid, microglial, PET imaging

INTRODUCTION

Alzheimer's disease (AD) is a progressive neurodegenerative disorder that afflicts over 35 million people throughout the world, including 5.8 million Americans age 65 and older [1]. Currently there is no effective disease-modifying therapy available to slow

*Correspondence to: David R. Elmaleh, 55 Fruit Street, Edw ards Research 015, Massachusetts General Hospital, Boston, MA 02114, USA. Tel.: +1 617 784 0480; E-mail: delmaleh@part ners.org. Georges El Fakhri, 125 Nashua Street, Boston, MA 02114, USA. Tel.: +1 617 724 6204; E-mail: elfakhri@pet.mgh. harvard.edu.

ISSN 1387-2877/$35.00

or stop the destruction of neurons that cause AD symptoms [2]. Present biochemical and pathological evidence support the concept that an imbalance between production and clearance of soluble amyloid-β ($A\beta_{42}$) resulting in abnormal accumulation of Aβ oligomers are responsible for the synaptotoxic effects that lead to neuronal stress, abnormal tau phosphorylation, synapse collapse, and memory impairment [3, 4]. Soluble Aβ monomers aggregate to form toxic higher order oligomers (dimers, trimers, up to dodecamers), which readily lead to extracellular deposition of fibrillar amyloid neuritic plaques that are resistant to degradation. Aβ oligomer accumulation drives tauopathy and neurodegeneration [5], all which combine to activate a microglial-driven neuroinflammatory response. Microglia are critical for Aβ phagocytosis; however, chronic inflammatory activation compromises microglial clearance of Aβ contributing to disease progression prior to clinical symptoms [6, 7]. Hence, interfering with the assembly of Aβ peptides from monomer to oligomeric species and fibrils, or promoting their clearance from the brain, are targets of anti-Aβ directed therapies in AD [8–10].

Microglia are the primary immune cells of the central nervous system (CNS) that play an important role in removal of cellular debris and aberrant protein debris. Microglial cells respond to the presence of AD pathological lesions (plaques and tangles) by changing their morphological characteristics, expressing numerous cell surface receptors, and surrounding the lesions [11–13]. Microglial cells can assume activation states in a spectrum ranging from phagocytic/neuroprotective to pro-neuroinflammatory. Under normal physiological conditions, microglia secrete anti-inflammatory cytokines and supportive growth factors for neuroprotection and neuro repair, while also clearing proteinaceous and cellular debris. Under pathological conditions, such as amyloid plaque accumulation, tauopathy and neurodegeneration in the AD brain, classically-activated microglia release toxic pro-inflammatory cytokines that induce gliosis dramatically amplify neurodegeneration. This process leads to more neuronal cell death and debris and accelerates disease progression. Research efforts have focused on converting microglia from the pro-neuroinflammatory activation state to the neuroprotective/anti-neuroinflammatory activation state in which the toxic effects are reduced and phagocytic activity toward Aβ is enhanced [14–17]. This is a potential avenue for new therapeutic approaches to treating and preventing AD.

Cromolyn (**1,** Fig. 1), also called cromolyn sodium, disodium cromoglycate, or hydroxy-cromolyn, is an FDA-approved drug originally introduced for the treatment of asthma [18]. Cromolyn is a synthetic chromone dimer derived from Khellin, a plant extract (*Ammi visnaga*) that was used to treat inflammatory diseases in ancient times [19]. This drug was shown to have lower toxicity in pure form compared to Khellin. Cromolyn is often characterized as a 'mast cell stabilizer' since it blocks allergen-induced bronchospasm presumably by inhibiting the release of inflammatory mediators from mast cells [20]. There is evidence that cromolyn also inhibits the inflammatory response of other cell types and thus it has been used for the treatment of diseases thought to involve mast cell activation, including allergic rhini-

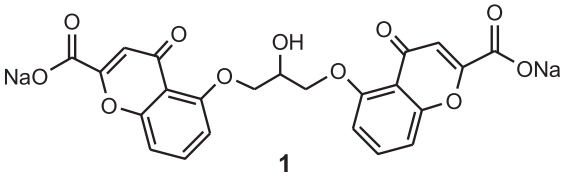

1

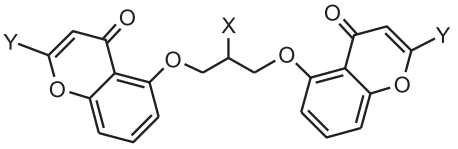

2-10

	X	Y
2	F	CO_2H
2a	^{18}F	CO_2H
3	OH	CO_2Et
4	F	CO_2Et
4a	^{18}F	CO_2Et
5	OH	CH_2OH
6	F	CH_2OH
7	OAc	CH_2OAc
8	OH	$CO_2CH_2O_2C^tBu$
9	F	$CO_2{}^tBu$
10	^{18}F	$CO_2{}^tBu$

Fig. 1. Cromolyn compounds.

tis, allergic conjunctivitis, and mastocytosis [21]. The underlying mechanism of action of cromolyn is not fully known; while cromolyn stabilizes mast cells, this mechanism does not fully explain its effect as an asthma medication [22]. Cromolyn is not restricted to antigen-evoked secretion, and some [23] have speculated that cromolyn may be a "membrane stabilizer" while others have suggested that it may facilitate closure of calcium channels in the mast cell membrane [24, 25]. Interestingly, cromolyn was found to inhibit the inflammatory processes in vivo in mast cell-deficient mice and to inhibit the activation of multiple hematopoietic cell types, including phagocytic cells other than mast cells *in vitro* [26].

Numerous studies indicate the involvement of chronic neuroinflammation in the pathogenesis of AD [2, 27]. The sustained activation of microglia and other immune cells in the brain release a variety of proinflammatory and toxic products, including reactive oxygen species, nitric oxide, and cytokines which exacerbate both amyloid and tau pathology. We have been investigating the potential utility of cromolyn as a therapeutic for slowing down AD progression and have reported that cromolyn inhibits Aβ aggregation, enhances microglial recruitment to plaques in transgenic AD mice, and promotes phagocytosis and clearance of Aβ [8, 28]. Cromolyn was found to efficiently inhibit the aggregation of Aβ monomers into higher order oligomers and fibrils *in vitro*, without affecting Aβ production; *in vivo*, the levels of soluble Aβ were decreased by over 50% after only 1 week of daily intraperitoneally administered cromolyn in *APP/PS1* AD mice [8]. This reduction in Aβ levels was largely attributed to the ability of cromolyn to promote microglial recruitment to Aβ plaques and to induce microglial phagocytosis of Aβ [28].

In a study of the effects of cromolyn on a the SO D1^{G93A} transgenic mouse model of familial amyotrophic lateral sclerosis, cromolyn treatment significantly delayed the onset of neurological symptoms, increased motor neuron survival in the lumbar spinal cord, and decreased the expression of pro-inflammatory cytokines/chemokines in the lumbar spinal cord and plasma. Together, these findings suggest that cromolyn sodium provides neuroprotection by decreasing neuroinflammatory response to disease pathology [29]. These neuroprotective mechanisms strongly suggest that cromolyn acts directly in the brain. To better understand the mechanism of action and to develop derivatives with enhanced brain penetration several fluoro-cromolyn derivatives have been investigated. Here, we report on the effect of fluoro-cromolyn derivatives on Aβ uptake by microglial cells, as well as microglial cell toxicity. We also describe the synthesis of F-18 labeled cromolyn analogs and their PET imaging pharmacokinetics in nonhuman primate brain.

MATERIALS AND METHODS

All experiments involving nonhuman primates were performed in accordance with the U.S. Department of Agriculture (USDA) Animal Welfare Act and Animal Welfare Regulations (Animal Care Blue Book), Code of Federal Regulations (CFR), Title 9, Chapter 1, Subchapter A, Part 2, Subpart C, §2.31. 2017. Experiments were approved by the Animal Care and Use Committee at the Massachusetts General Hospital. The animal used in this study was an adult male Rhesus macaque (13 years old). Prior to each study, animals were sedated with ketamine/xylazine (10/0.5 mg/kg IM) and were intubated for maintenance anesthesia with isoflurane (1-2% in 100% O_2). A venous catheter was placed for infusion of the radiotracer and, where applicable, an arterial catheter was placed for sampling of the arterial input function. The animal was then positioned on a heating pad on the bed of the scanner for the duration of the study.

A GE PETtrace 16.5 MeV cyclotron (GE Healthcare, Waukesha, WI, USA) was used for [^{18}F]fluoride production by the ^{18}O(p,n)^{18}F nuclear reaction to irradiate ^{18}O-enriched water (Isoflex Isotope, San Francisco, CA). Dynamic PET sinograms were performed on a GE Discovery MI (GE Healthcare) PET/CT scanner.

Chemistry

Hydroxy-cromolyn **1** (cromolyn sodium) was purchased from Quotient Sciences (Nottingham, UK) or Millipore Sigma (St. Louis, USA). All cromolyn derivatives were synthesized and fully characterized (Supplemental Material). Log *P* values for **4a** and **10** were determined according to the following procedure. An aliquot (10 μL, 74 kBq) of the F-18 tracer was added to a test tube containing 2.5 mL of octanol and 2.5 mL of phosphate buffer solution (pH 7.4). The test tube was mixed by vortex for 2 min and then centrifuged for 2 min to fully separate the aqueous and organic phase. The samples taken from the octanol layer (0.1 mL) and the aqueous layer (1.0 mL) were saved for radioactivity measurement. An additional aliquot of the octanol layer (2.0 mL) was transferred to a new test tube containing 0.5 mL of octanol

and 2.5 mL of phosphate buffer solution (pH 7.4). The previous procedure (vortex mixing, centrifugation, sampling, and transfer to the next test tube) was repeated until six sets of aliquot samples had been prepared. The radioactivity of each sample was measured using PerkinElmer Wizard2 2480 gamma-counter. The log *P* values of each set of samples were calculated as Log D7.4 = Log (radioactivity of octanol layer × 10 / radioactivity of PBS layer).

Preparation of cromolyn derivatives for microglial cell-based assays

Cromolyn derivatives, **3** and **4**, displayed lower solubility in DMSO in comparison to **1**, **2**, **5**, and **6**–**8**. Therefore, we generated 25 mM stock solutions for all the compounds except for **3** and **4**. The stock solutions for **3** and **4** were prepared at 5 mM and 7.5 mM, respectively.

Generation of the single cell clone BV2 microglial line stably expressing human CD33 (BV2-CD33^{WT})

To generate a single cell clone BV2 line stably expressing human CD33, a well of a 6-well-plate containing naive BV2 cells were transiently transfected with the pcDNA3.1 plasmid encoding human wild-type CD33 (CD33^{WT}) using Lipofectamine-Plus (Life Technologies), according to the manufacturer's instructions. The following day the media was changed. Two days post transfection, we started the process of isolating a clonal population of BV2 cells stably expressing CD33^{WT}. For this purpose, cells were trypsinized and centrifuged. Afterwards, cells were washed with phosphate buffer saline (PBS) and centrifuged. The cell pellet was resuspended in FACS sorting buffer that consists of 2% heat-inactivated fetal bovine serum, 2% B27 supplement (Gibco) in PBS. Subsequently, cells were incubated in FACS sorting buffer containing Fc block (1 μg/ml, anti-mouse CD16/32, clone 93, Biolegend) for 10 min on ice. Afterwards, cells were labeled with either anti-CD33 antibody-FITC (mouse IgG1, clone HIM3-4, BD Pharmingen) or IgG1-FITC (BD Pharmingen) as control for 30 min on ice. Cells were rinsed with FACS sorting buffer and centrifuged. Then, cells were gently resuspended in FACS sorting buffer and filtered into polystyrene filter top tubes (BD Falcon) for FACS sorting.

BV2 cells expressing CD33^{WT} were visualized based on CD33 expression, using FACS ARIA (BD Biosciences). The anti-CD33 antibody-FITC bound to CD33 expressed on the cell surface, while cells treated with the isotype antibody IgG1 served as control. Single cells were sorted based on the expression levels of CD33 detected in the FITC channel, using FACS ARIA. Single cells were sorted into 96-well plates containing cell growth media: DMEM (Lonza), 10% heat-inactivated fetal bovine serum, 2 mM L-glutamine, 1% penicillin/streptomycin, and geneticin at 400 μg/ml (G418 sulfate, Life Technologies). The pcDNA3.1-CD33^{WT} vector contains the neomycin resistance gene for selection of stable cell lines using geneticin. After one week, half of the cell growth media was replaced with fresh media in each well every three days. After an additional week, each single cell clone was trypsinized and transferred into one well in 24-well plates for cell expansion. Upon reaching confluency, each single cell clone was trypsinized and plated into two wells in 6-well plates. Once confluent, cells from one well were frozen in heat-inactivated fetal bovine serum containing 10% dimethyl sulfoxide (Sigma Aldrich), while cells in the second well were lysed in RIPA lysis buffer (EMD Millipore) supplemented with protease inhibitors (Roche) and phosphatase inhibitors (Thermo Fisher Scientific). We obtained several cell clones that we screened for CD33 expression by using western blotting and anti-human CD33 antibody (mouse monoclonal, clone PWS44, Leica Biosystems). Finally, the single cell clone line expressing CD33^{WT} (BV2-CD33^{WT}) was identified and confirmed by western blotting. The corresponding frozen cell vial was rapidly thawed and plated in cell growth media in a 10 cm culture dish to allow cell expansion.

Cromolyn compounds microglial toxicity and Aβ uptake assays in microglia

Naive BV2 microglial cell line or single cell clone BV2 line stably expressing CD33^{WT} (BV2-CD33^{WT}) were plated in 12-well plates at the density of 5x10E5 cells for naïve BV2 and 7x10E5 cells for the BV2-CD33^{WT} cell clone, in proliferating media: DMEM containing 10% heat-inactivated fetal bovine serum, 2 mM L-Glutamine and 1% penicillin/streptomycin (Life Technologies). On the following day, cells were treated with DMSO (control) or cromolyn derivatives at different concentrations in proliferating media for 3 h. **1**, **2**, **5**, and **6**–**8** were tested at 10, 50, 100, and 150 μM, while **3** and **4** were assessed at 5, 25, 50, and 75 μM due to solubility limit in DMSO. Afterwards, cells were washed twice with PBS and

treated with cromolyn derivatives or DMSO (control) in the presence of soluble untagged $A\beta_{42}$ peptide (400 nM) in DMEM media for 2 h. At the end of the treatment, cell media was collected and compound toxicity was assessed with CytoTox-ONE™ lactate dehydrogenase (LDH) assay. LDH is a cytosolic enzyme present in many different cell types that is released after cell death and disruption and is a well-established indicator of cellular toxicity. Remaining cells in the plate were washed three times with cold PBS and lysed with RIPA buffer (EMD Millipore) supplemented with protease inhibitors (Roche) and phosphatase inhibitors (Thermo Fisher Scientific). Protein concentrations in the lysate supernatants were determined using the Pierce™ BCA protein assay kit and 2-3 μg/well of total protein from each lysate was analyzed for $A\beta_{42}$ uptake using the $A\beta_{42}$ ELISA kit from Wako. $A\beta_{42}$ levels were normalized to total protein concentration. Toxic compound concentrations were excluded from the $A\beta_{42}$ analysis and further studies.

PET imaging

A CT scan was acquired for attenuation correction of the PET images. Emission PET data collection was initiated after bolus injection of F-18 cromolyn derivatives (207.2 MBq) into the lateral saphenous vein of a rhesus macaque followed by a saline flush. Dynamic PET imaging was performed for up to 180 min with arterial blood sampling. Total volume of distribution (vt) was estimated using compartmental modeling (one- and two-tissue configurations) and graphical analysis techniques (Logan regression methods). Time bins were 6×10, 8×15, 6×30, 8×60, 8×120, and 30×300 s for 18F-TS274 and 6×10, 8×15, 6×30, 8×60, 8×120, and 18×300 s. Imaging started at the same time as bolus injection. Dynamic PET sinograms were reconstructed using the VPFXS reconstruction with 34 subsets and 3 iterations. Final reconstructed images had voxel dimensions of 256×256×89 and voxel sizes of 1.7×1.7×2.8 mm. The GE discovery MI scanner used for these studies has a spatial resolution around 5 mm at the center of the field of view. Dynamic PET sinograms were reconstructed using the VPFXS reconstruction with 34 subsets and 3 iterations. Final reconstructed images had voxel dimensions of 256×256×89 and voxel sizes of 1.7×1.7×2.8 mm. The GE discovery MI scanner used for these studies has a spatial resolution around 5 mm at the center of the field of view.

Whole blood and plasma time-activity curves were obtained by linear interpolation of radioactivity concentrations (kBq/cc) measured from the arterial blood samples. Blood samples were drawn at different time points during the entire experiment. Arterial samples of 1–3 mL were acquired every 30 s immediately following radiotracer injection during the first 5 min and decreased in frequency to every minute, 2 min, 5 min, 15 min, and 30 min toward the end of the scanning duration. Metabolite analysis was performed on standard and the plasma samples drawn at 5, 10, 15,

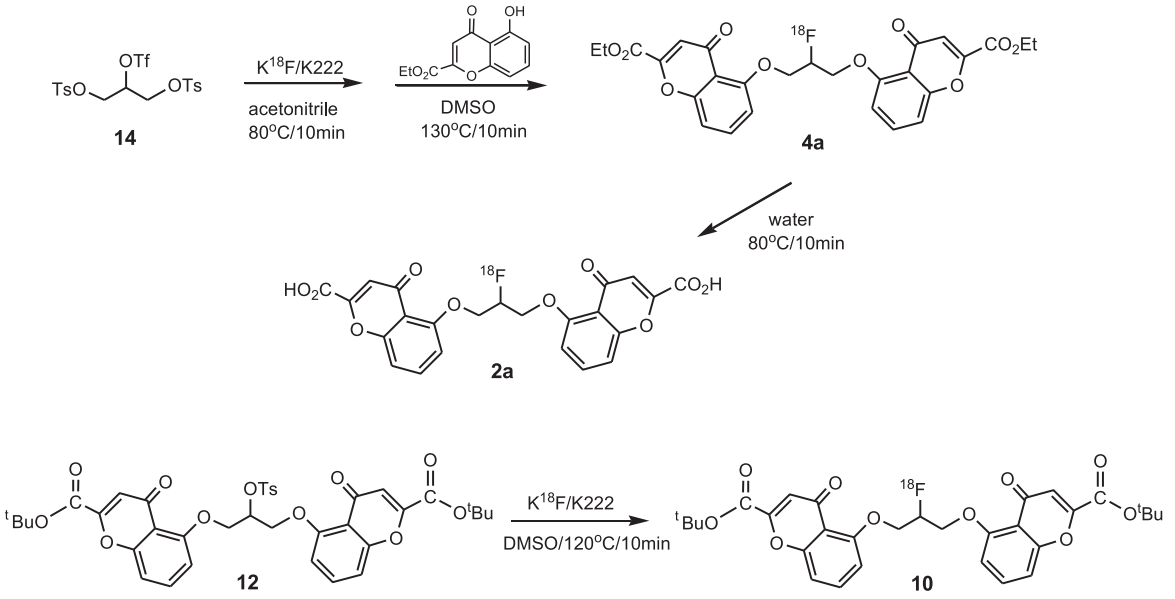

Scheme 1. Radiosynthesis of **4a**, **2a**, and **10**.

30, 60, 90, 120, and 180 min. These samples were assayed with column-switching radio-HPLC to determine the fraction of total radioactivity that was attributable to intact radiotracer. Plasma protein binding was measured in blood drawn immediately prior to tracer injection.

Radiofluorination

5, 5'- [(2-[^{18}F]Fluoro- 1, 3-propanediyl) bis(oxy)] bis[4- oxo-4H- 1- benzopyran- 2- carboxylic acid diethyl ester] (4a)

A [^{18}F]fluoride solution (50 mCi) was trapped onto a QMA Sep-Pak Cartridge (Sep-Pak plus light, Waters, Milford, MA) and then released by a solution of Kryptofix-2.2.2. (6 mg) and potassium carbonate (2 mg) in acetonitrile and water (1 mL, v/v 7:3) into a sealed Wheaton 5 mL reaction vial. The [^{18}F] fluoride solution was azeotropically dried with the aid of nitrogen gas at 120°C for 10 min. The K^{18}F/Kryptofix complex was dried three times at 120°C by the addition of 1 mL of acetonitrile followed by evaporation of the solvent using a nitrogen flow. A solution of 1,3-bis[tolylsulfonyl)oxy]-2-[(trifluoromethyl)-sulfonyl]oxy-propane (4 mg, **14**) in anhydrous acetonitrile was added to the vial and fluorination was performed at 80°C for 10 min. The resultant 2-[^{18}F] fluoropropane 1,3-ditosylate solution (90%, radio-TLC) was passed through a silica gel SepPak using methylene chloride into a vial containing K_2CO_3 (10 mg) and ethyl 5-hydroxy-4-oxo-4H-chromene-2-carboxylate (10 mg) (Sigma-Aldrich). After solvent removal, anhydrous DMSO (0.8 mL) was added and the mixture was heated for 10 min at 130°C. Once cooled to 25°C, 1 mL of 5% HCl, followed by 2 mL of 50/50 acetonitrile 0.1 M ammonium formate was added and the mixture was filtered (Millex-LCR 0.45 μm). F-18 cromolyn diester **4a** was purified by HPLC (Phenomenex Luna C18, 250 × 10 mm, 50:50 acetonitrile/0.1 M ammonium formate (pH 6.0). The fraction containing **4a** was diluted with water (30 mL) and loaded onto a C-18 Sep-Pak (Waters, Milford, MA). Finally, the cartridge was washed with water (5 mL) and **4a** was eluted with ethanol (1 mL), diluted with saline to a final 10% ethanol/saline solution and filtered (0.22u Millex-GV). Synthesis was complete within 90 min and chemical purity was greater than 95% (5 mCi, 20 ± 5% EOB, $n = 10$). The molar activity, radiochemical identity and purity of injected **4a** were determined by an analytical HPLC system using an analytical column (Waters, XBridge, C18, 3.5 μ, 4.6×150 mm) with a mobile phase of acetonitrile/0.1M aqueous ammonium formate solution (60/40, v/v) at a flow rate of 1 mL/min and UV absorption at λ = 254 nm.

5, 5'- [(2-[^{18}F]Fluoro- 1, 3- propanediyl) bis(oxy)] bis[4- oxo-4H- 1- benzopyran- 2- carboxylic acid] (2a)

Following the procedure for the synthesis of **4a**, water (1 mL) was added in place of HCl at the completion of the final step and the mixture was heated at 80°C for 10 min. Once cooled to 25°C, 1 mL of 50/50 acetonitrile 0.1 M ammonium formate was added and the mixture was filtered (Millex-LCR 0.45 μm). F-18 cromolyn diacid **2a** was purified by HPLC (Phenomenex Luna C18, 250 x 10 mm, 10:90 acetonitrile/0.1 M ammonium formate). The fraction containing F-18 cromolyn diacid was diluted with water (30 mL) and loaded onto a C-18 Sep-Pak and the cartridge was washed with water (5 mL) and activity was eluted with ethanol (1 mL), diluted with saline to final a 10% ethanol/saline solution and filtered (0.22u Millex-GV). Synthesis was complete within 90 min and chemical purity was greater than 95%. (14 ± 5% EOB, $n = 10$).

5, 5'-(2-[^{18}F] Fluoro- 1, 3- propanediyl) bis(oxy)] bis[4- oxo-4H- 1- benzopyran- 2- carboxylic acid di-tert-butyl ester] (10)

A sealed Wheaton 5 mL reaction vial containing 50 mCi of fluorine–18 in 1 mL of ^{18}O-enriched water, Kryptofix-2.2.2. (6 mg), and potassium carbonate (2 mg) was heated at 120°C and solvent was evaporated with the aid of nitrogen gas. The K^{18}F/Kryptofix complex was dried three times at 120°C by the addition of 1 mL of acetonitrile followed by evaporation of the solvent using a nitrogen flow. A solution of the tosylate cromolyn t-butyl diester **12** (5 mg) in DM SO (0.7 mL) was added to the vial and fluorination was performed at 120°C for 10 min. Once cooled to 25°C, 2 mL of 50/50 acetonitrile 0.1 M ammonium formate was added and. F-18 cromolyn t-butyl diester **10** was purified by HPLC (Phenomenex Luna C18, 250 × 10 mm, 50:50 acetonitrile/0.1 M ammonium formate). The fraction containing F-18 cromolyn diester **10** was diluted with water (30 mL) and loaded onto a C-18 Sep-Pak and the cartridge was washed with water (5 mL) and activity was eluted with ethanol (1 mL) into a vial, diluted with saline to final 10% ethanol/saline solution and filtered (0.22u Millex-GV). Synthesis was complete within 90 min and chemical purity was greater than 95%. (10% EOB)

RESULTS

Cromolyn microglial cell toxicity

Naive BV2 microglial cells were treated with DMSO (control) or hydroxy-cromolyn **1** or cromolyn derivatives (**2**–**8**) for 3 h at different concentrations. Afterwards, cells were incubated with soluble untagged Aβ_{42} peptide and DMSO or cromolyn derivatives for 2 h. At the end of the treatment, cell media was collected, and compound toxicity was assessed with the lactate dehydrogenase (LDH) assay. All compounds but one exhibited very low microglial cell toxicity at 10 to 150 μM concentrations (Fig. 2). BV2 microglial cells treated with the cromolyn derivative **8**, originally designed as a prodrug to deliver **1** through the skin [30], exhibited increased toxicity at 100 and 150 μM in comparison to cells treated with the vehicle (DMSO) (see Fig. 4). Toxic compound concentrations were excluded from the Aβ_{42} analysis and further studies.

Cromolyn derivative effect on microglial uptake of Aβ_{42}

To explore the effects of cromolyn derivatives on Aβ_{42} uptake, we employed a microglial cell-based assay. Specifically, naïve BV2 microglial cell cultures were treated with cromolyn derivatives **1**–**8** at different concentrations ranging between 5 and 150 μM for 3 h. Subsequently, cells were incubated with soluble Aβ_{42} and cromolyn derivatives for 2 h. After incubation, cells were collected for ELISA analysis to measure Aβ_{42} levels. Cromolyn **1** (hydroxy cromolyn) and cromolyn derivative **2** led to a modest increase of Aβ_{42} uptake at 100 and 150 μM and 10 and 100 μM, respectively in BV2 cells. Interestingly, the cromolyn derivative **6** led to a robust inhibition of Aβ_{42} uptake in BV2 microglial cells (Fig. 3). Remarkably, we found that the cromolyn derivative **4** is the most effective and at 75 μM leads to a significantly increased uptake of Aβ_{42} in BV2 microglial cells in comparison to vehicle treatment.

We previously showed that the AD risk factor *CD33* inhibits uptake and clearance of Aβ_{42} in microglial cell cultures, a process that requires the sialic acid-binding V-Ig domain of CD33 [31]. Here, we generated a single cell clone BV2 line stably expressing human wild-type CD33 (BV2-CD33^{WT}). The effect of cromolyn derivatives on microglial uptake and clearance of Aβ_{42} was investigated in the single cell clone BV2-CD33^{WT} microglial line. BV2-CD33^{WT} cells were treated with DMSO (control) or cromolyn derivatives at different concentrations

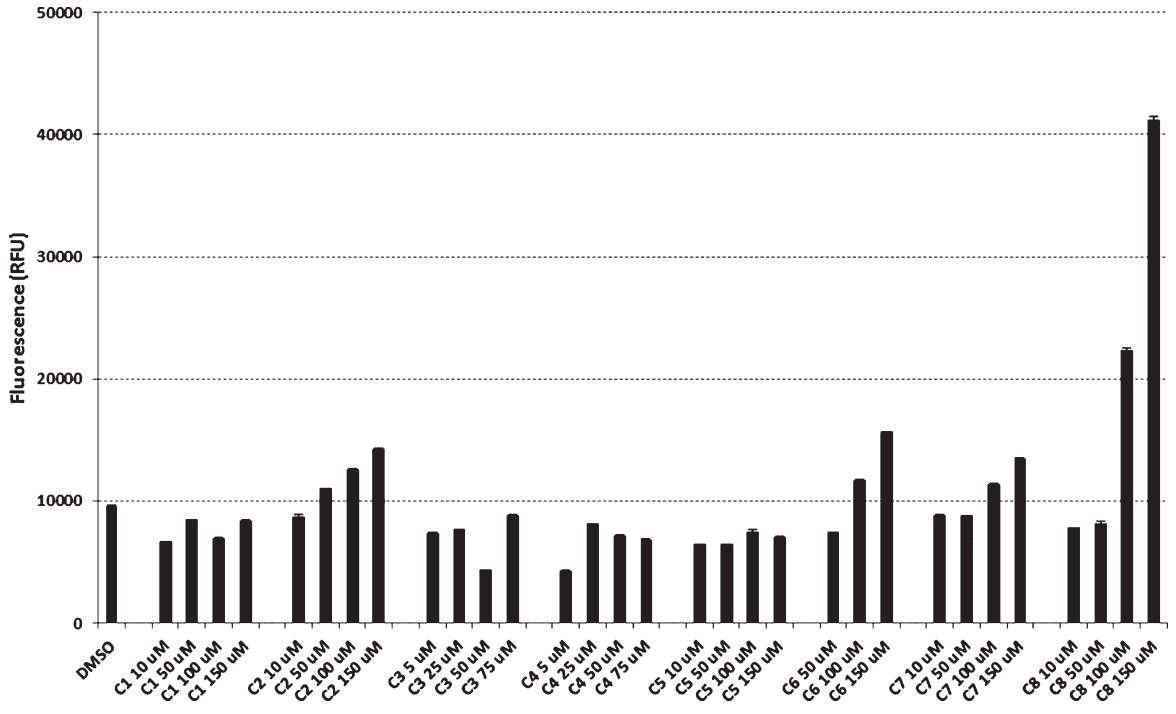

Fig. 2. Microglial toxicity of cromolyn derivatives compared to DMSO.

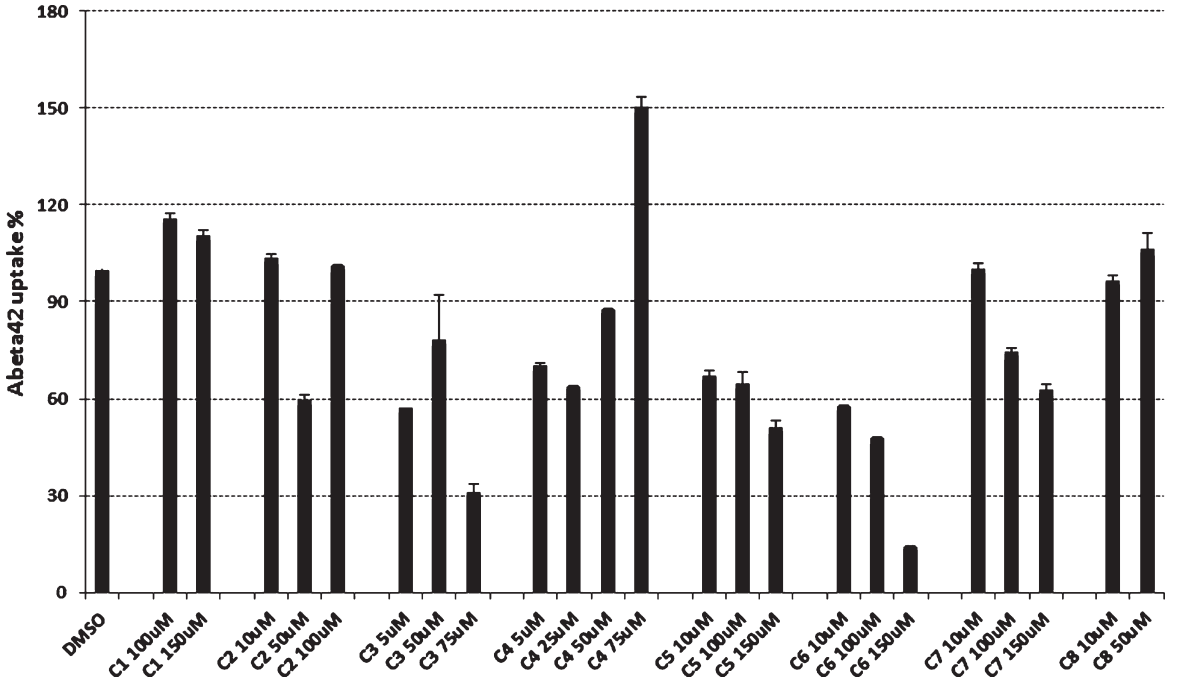

Fig. 3. Effect of cromolyn derivatives on $A\beta_{42}$ uptake in naïve BV2 microglial cells.

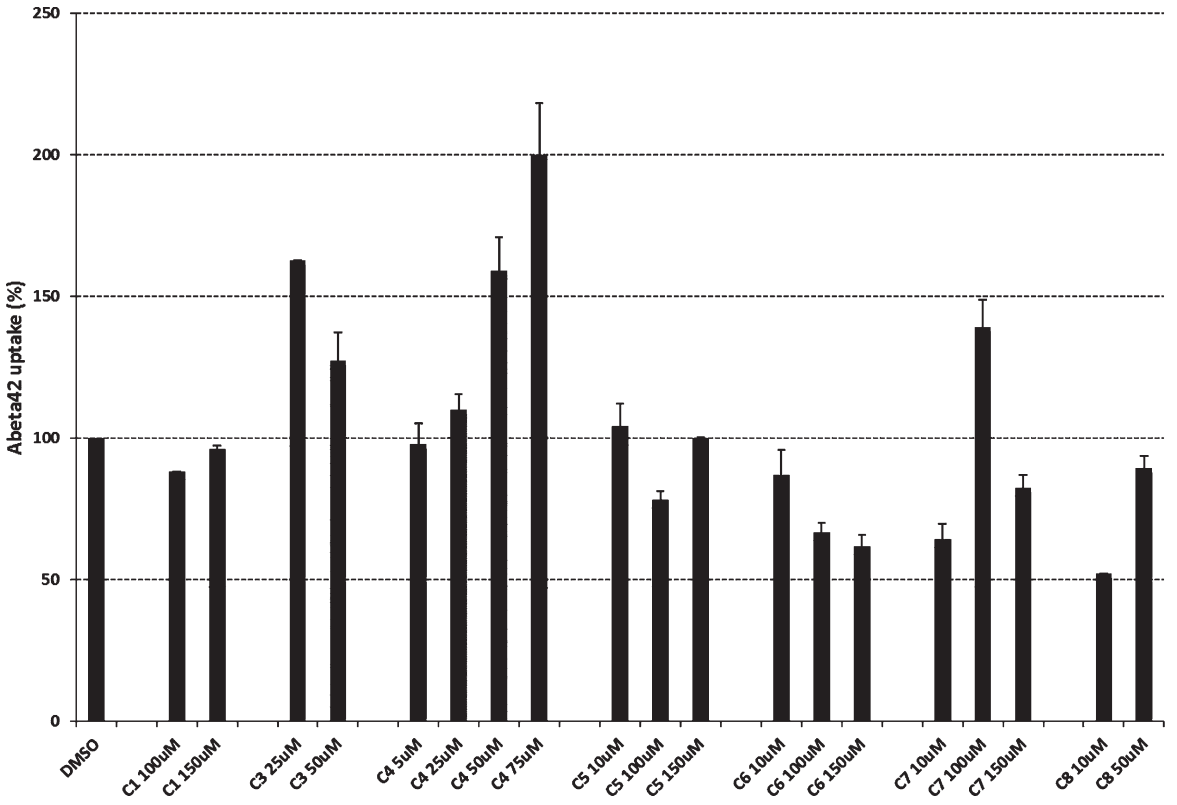

Fig. 4. Effect of cromolyn derivatives on $A\beta_{42}$ uptake in microglial BV2-$CD33^{WT}$ activated cells.

ranging between 5 and 150 μM. Results for compounds **3**, **4**, and **7** impacted microglial uptakes of $A\beta_{42}$ at the concentrations tested in comparison to DMSO. We also showed that cromolyn derivative **6** inhibits negative uptake of $A\beta_{42}$ in BV2-CD33^{WT} cells as compared to DMSO treatment (Figs. 3 and 4). Using the GraphPad Prism 7 software, the IC_{50} for fluoro-cromolyn diethyl ester **4** was 54.7 μM in BV2-CD33^{WT} cells.

Radiofluorination

Radiosynthesis of cromolyn **2a** and **4a** was achieved in a two-step process due to susceptibly of the of the diethyl ester precursor to hydrolysis at reaction temperatures above 120°C. Fluorine-18 labeling of the cromolyn diethyl ester tosylate or mesylate using either potassium carbonate or potassium bicarbonate and Kryptofix-2.2.2 or using tetrabutylammonium bicarbonate in DMSO at temperatures between 120°C-140°C gave 0 to 5% yield of **4a**. In contrast, the two-step method provided **4a** in an overall yield of 20%, consistently. This was possible due to the selective displacement of the triflate moiety in 1, 3-bis[tolylsulfonyl)-oxy]-2-[(trifluoromethyl)-sulfonyl]oxypropane (**14**) with fluorine-18 at 80°C in acetonitrile. Radiofluorination of the tosylate of cromolyn di-*tert*-butyl ester (**12**) to provide **10** did not undergo substantial hydrolysis during labeling conditions with potassium carbonate/Kryptofix-2.2.2.

PET imaging

The aim of this PET study was to measure brain exposure and regional distribution of selected F-18 labeled cromolyn analogs administered intravenously in a monkey with an intact BBB. Pharmacokinetics of three F-18 analogs (diethyl ester **4a**, di-tert-butyl ester **10**, and diacid **2a**) were determined by dynamic PET imaging in a rhesus macaque monkey. Arterial blood sampling and radio-metabolite analysis was also performed. PET imaging revealed the order of brain tracer penetration to be diethyl ester **4a**>di-tert-butyl ester **10**> diacid **2** (Figs. 5 and 6). The brain distribution of diacid **2a** matched the cerebral blood volume, suggesting negligible BBB penetration at tracer levels.

PET images obtained with [^{18}F]fluoro-cromolyn diethyl ester **4a** showed enhanced uptake in areas of high perfusion (putamen, grey matter and cerebellum) and lower signal in areas of lower perfusion (caudate, thalamus, and white matter) (Fig. 5). Brain penetration was immediate, reaching maximum at 2 min (2.3 SUV) and washout was slow, 2 SUV at

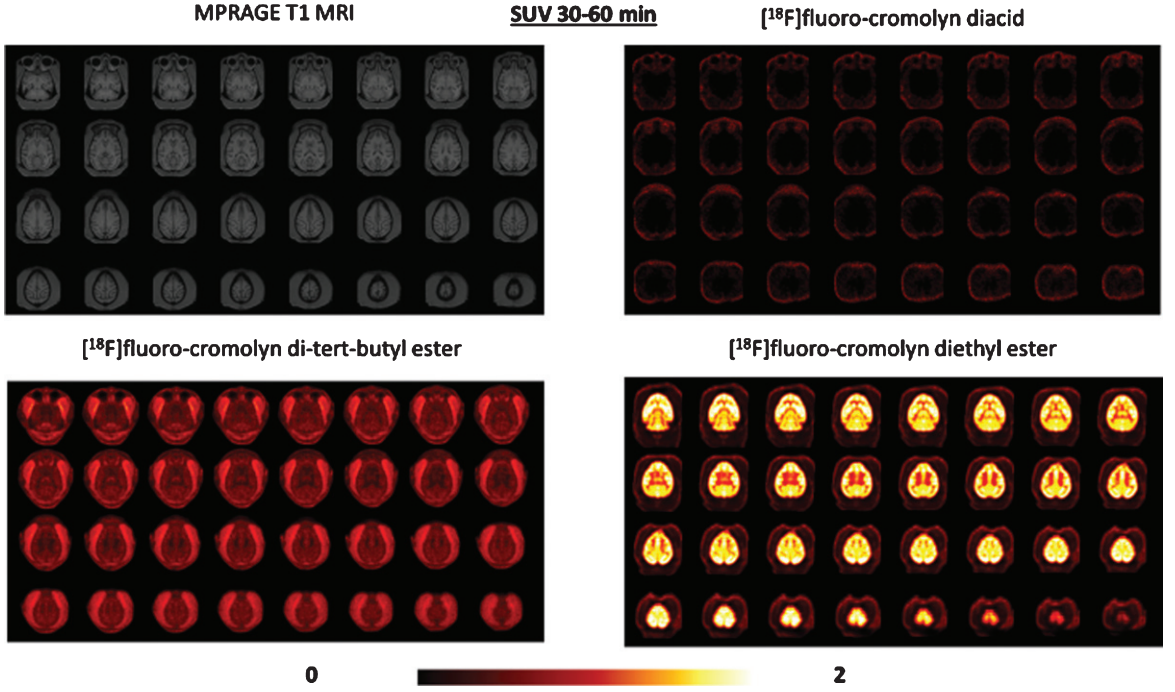

Fig. 5. PET imaging data comparison of [^{18}F]fluoro-cromolyn diacid **2a** (top right), [^{18}F]fluoro-cromolyn di-tert-butyl ester **10** (bottom left) and [^{18}F]fluoro-cromolyn diethyl ester **4a** (bottom right) in monkey.

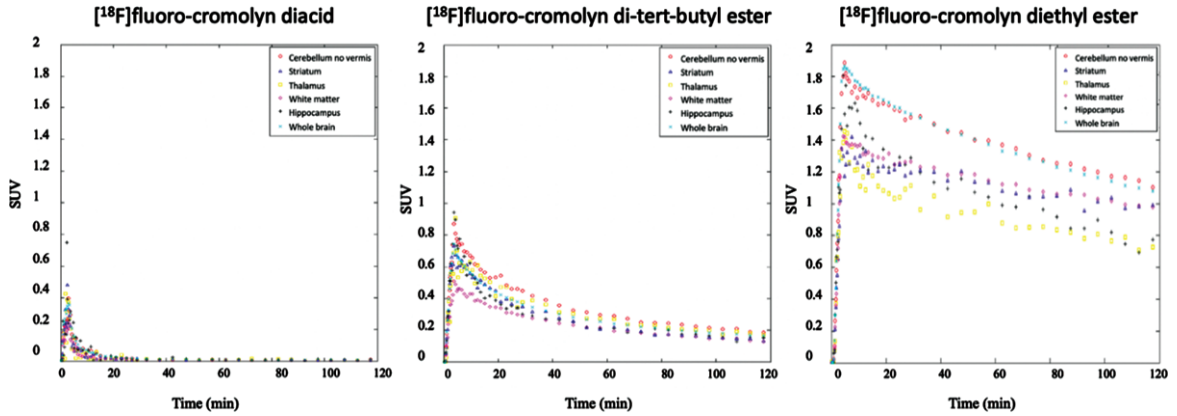

Fig. 6. Time-activity curves from PET imaging data of [^{18}F]fluoro-cromolyn diacid **2a**, [^{18}F]fluoro-cromolyn di-tert-butyl ester **10** and [^{18}F]fluoro-cromolyn diethyl ester **4a** in monkey.

20 min, 1.5 at 60 min (Fig. 6). Blood sampling for this study revealed ^{18}F-diacid cromolyn as the only metabolite (20–140 min). Hydrolysis to form [^{18}F] fluoro-cromolyn diacid **2a** appears to take place in the blood as evidenced by *ex vivo* stability tests. The t-butyl ester derivative **10** also metabolized to the ^{18}F-diacid, albeit, more slowly.

DISCUSSION

Our results indicate that fluoro-cromolyn derivatives represent potential therapeutic agents for treating and preventing AD by reducing pro-neuroinflammatory activation of microglia, enhancing microglial phagocytosis and promoting clearance of Aβ. Several fluoro-cromolyn and non-fluoro-cromolyn derivatives were investigated in this initial screening to better understand the structure-activity relationship of cromolyn to microglial uptake and clearance of $A\beta_{42}$ and to develop derivatives with enhanced brain penetration. Replacement of OH in cromolyn by F and esterification of the acid or reduction to the alcohol are expected to result in enhanced lipophilicity and thus greater brain permeable compounds. Moreover, fluorine derivatives offer the added advantage of monitoring brain penetration by labeling with flourine-18 and using PET imaging. Additionally, cromolyn derivatives containing labile substituents such as ethyl ester, t-butyl ester, acetate or methyl pivalate ester could act as lipophilic transient derivatives or prodrugs to deliver cromolyn **1**, **2**, **5**, or **6** to the brain. Substitution of the hydroxyl group in **1** for fluoride did not significantly alter microglial uptake of $A\beta_{42}$ based on comparable results obtained with **2** (Fig. 3). However, substitution of the hydroxyl group for fluoride in diethyl ester **3** did show an increase in microglial uptake of $A\beta_{42}$ based on comparable results obtained with **4** at 75 μM (Fig. 4). Interestingly, replacing carboxyl groups with hydroxymethyls as in **5** and **6** negatively impacted microglial uptake of $A\beta_{42}$ indicating the possible significance of this moiety in the binding mechanism. Although, it must be noted that triacetate **7** derived from hydroxymethyl **5** exhibited a less negative impact of microglial uptake of $A\beta_{42}$ in BV2 microglial cells (Fig. 3) and had a positive impact of microglial uptake of $A\beta_{42}$ in BV2-CD33 activated microglial cells at 100 μM (Fig. 4). This increase microglial uptake of $A\beta_{42}$ may be due to the presence of acetyl groups on **7**. Remarkably, fluoro-cromolyn diethyl ester **4** increased microglial uptake of $A\beta_{42}$ in a dose-dependent manner and at 75 μM resulted in a one-fold increase in $A\beta_{42}$ uptake in BV2-CD33^{WT}. The IC_{50} for fluoro-cromolyn diethyl ester **4** was found to be 54.7 μM in BV2-CD33^{WT} cells. These results suggest that fluoro-cromolyn diethyl ester **4** promotes microglial uptake and clearance of $A\beta_{42}$ by pharmacologically converting microglial cells from neurotoxic/pro-inflammatory activation to a more beneficial neuroprotective/pro-phagocytic activation state.

PET imaging with three [^{18}F]fluoro-cromolyn derivatives revealed the order of brain tracer penetration to be diethyl ester **4a** > di-tert-butyl ester **10** > diacid **2** (Figs. 5 and 6). Brain uptake corresponded to lipophilicity values where the measured logP value for the diethyl ester was 2.2 compared to the di-tert-butyl with a measured value of 3.2 that is slightly above the range for ideal blood-brain barrier (BBB)

penetration. BBB penetration is optimal when LogP values are in the range of 1.5–2.7 with a mean value of 2.1 [31]. The brain distribution of diacid **2a** matched the cerebral blood volume, suggesting negligible BBB penetration at tracer levels. However, it must be noted that administration of hydroxy-cromolyn **1** in typical drug doses by either oral inhalation (17.1 mg) or i.p. injection (25 mg/kg) results in detectable brain uptake [7, 32]. PET images obtained with [^{18}F]fluoro-cromolyn diethyl ester **4a** showed enhanced uptake in areas of high perfusion (putamen, grey matter, and cerebellum) and lower signal in areas of lower perfusion (caudate, thalamus, and white matter) (Fig. 5). Brain penetration was immediate, reaching maximum at 2 min and washout was slow. Metabolite analysis of both diethyl **4a** and di-*tert*-butyl **10** derivatives revealed that these compounds hydrolyze to diacid **2a**. These findings indicate that [^{18}F]fluoro-cromolyn diethyl ester **4a** readily enters the brain whereupon it hydrolyzes to [^{18}F]fluoro-cromolyn diacid **2a** and is accumulated in the brain. This can be a method to deliver **2a** into the brain following i.v. administration of [^{18}F]fluoro-cromolyn diethyl ester **4a** to determine regional distribution. Unfortunately, for use as a therapeutic drug, the rate of hydrolysis or short half-life of **4** *in vivo* needs to be addressed. Development of a controlled-release formulation or oral inhalation delivery of cromolyn **4** for optimal bioavailability is one approach. Another strategy is to screen cromolyn derivatives and prodrugs that are less prone to hydrolysis but still maintain optimal therapeutic performance.

In summary, these results indicate that fluoro-cromolyn derivatives represent potential therapeutic agents for treating and preventing AD by reducing pro-neuroinflammatory activation of microglia and simultaneously promoting clearance of Aβ via microglial phagocytosis.

ACKNOWLEDGMENTS

This study was funded by the Gordon Center for Medical Imaging NIH Grant: P41EB022544 TDR3.

Authors' disclosures available online (https://www.j-alz.com/manuscript-disclosures/20-1419r1).

SUPPLEMENTARY MATERIAL

The supplementary material is available in the electronic version of this article: https://dx.doi.org/10.3233/JAD-201419

REFERENCES

[1] (2020) 2020 Alzheimer's disease facts and figures. *Alzheimers Dement* **16**, 391-460.

[2] Kinney JW, Bemiller SM, Murtishaw AS, Leisgang AM, Salazar AM, Lamb BT (2018) Inflammation as a central mechanism in Alzheimer's disease. *Alzheimers Dement (N Y)* **4**, 575-590.

[3] Selkoe DJ, Hardy J (2016) The amyloid hypothesis of Alzheimer's disease at 25 years. *EMBO Mol Med* **8**, 595-608.

[4] Larson ME, Lesné SE (2012) Soluble Aβ oligomer production and toxicity. *J Neurochem* **120**(Suppl 1), 125-139.

[5] Choi SH, Kim YH, Hebisch M, Sliwinski C, Lee S, D'Avanzo C, Chen J, Hooli B, Asselin C, Muffat J, Klee JB, Zhang C, Wainger BJ, Peitz M, Kovacs DM, Woolf CJ, Wagner SL, Tanzi RE, Kim DY (2014) A three-dimensional human neural cell culture model of Alzheimer's disease. *Nature* **515**, 274-278.

[6] Rogers J, Lue LF (2001) Microglial chemotaxis, activation, and phagocytosis of amyloid beta-peptide as linked phenomena in Alzheimer's disease. *Neurochem Int* **39**, 333-340.

[7] Yamanaka M, Ishikawa T, Griep A, Axt D, Kummer MP, Heneka MT (2012) PPARγ/RXRα-induced and CD36-mediated microglial amyloid-β phagocytosis results in cognitive improvement in amyloid precursor protein/presenilin 1 mice. *J Neurosci* **32**, 17321-17331.

[8] Y Hori, S Takeda, H Cho, S Wegmann, TM Shoup, K Takahashi, D Irimia, DR Elmaleh, BT Hyman, E Hudry (2015) FDA approved asthma therapeutic agent impacts Aβ in the brain in a transgenic model of Alzheimer's disease *J Biol Chem* **290**, 1966-1978.

[9] Jamasbi E, Wade JD, Separovic F, Hossain MA (2016) Amyloid beta (Aβ) peptide and factors that play important roles in Alzheimer's disease. *Curr Med Chem* **23**, 884-892.

[10] Yasumoto T, Takamura Y, Tsuji M, Watanabe-Nakayama T, Kmamura K, Inoue H, Nakamura S, Inoue T, Kimura A, Yano S, Nishijo H, Kiuchi Y, Teplow DB, Ono K (2019) High molecular weight amyloid β1-42 oligomers induce neurotoxicity via plasma membrane damage. *FASEB J* **3**, 9220-9234.

[11] Thériault P, ElAli A, Rivest S (2015) The dynamics of monocytes and microglia in Alzheimer's disease. *Alzheimers Res Ther* **7**, 41-51.

[12] Wilcock DM (2012) A changing perspective on the role of neuroinflammation in Alzheimer's disease. *Int J Alzheimers Dis* **2012**, 495243.

[13] McGeer P, McGeer E (2010) Targeting microglia for the treatment of Alzheimer's disease. *Expert Opin Ther Targets* **19**, 497-506.

[14] Mandrekar S, Landreth GE (2010) Microglia and inflammation in Alzheimer's disease. *CNS Neurol Disord Drug Targets* **9**, 156-167.

[15] Rubio-Perez JM, Morillas-Ruiz JM (2012) A review: Inflammatory process in Alzheimer's disease, role of cytokines. *ScientificWorldJournal* **2012**, 756357.

[16] Akiyama H, Barger S, Barnum S, Bradt B, Bauer J, Cole GM, Cooper NR, Eikelenboom P, Emmerling M, Fiebich BL, Finch CE, Frautschy S, Griffin WS, Hampel H, Hull M, Landreth G, Lue L, Mrak R, Mackenzie IR, McGeer PL, O'Banion MK, Pachter J, Pasinetti G, Plata-Salaman C, Rogers J, Rydel R, Shen Y, Streit W, Strohmeyer R, Tooyoma I, Van Muiswinkel FL, Veerhuis R, Walker D, Webster S, Wegrzyniak B, Wenk G, Wyss-Coray T (2000)

Inflammation and Alzheimer's disease. *Neurobiol Aging* **21**, 383-421.

[17] Liu S, Liu Y, Hao W, Wolf L, Kiliaan AJ, Penke B, Rübe CE, Walter J, Heneka MT, Hartmann T, Menger MD, Fassbender K (2012) TLR2 is a primary receptor for Alzheimer's amyloid β peptide to trigger neuroinflammatory activation. *J Immunol* **188**, 1098-1107.

[18] Altounyan REC (1967) Inhibition of experimental asthma by a new compound-disodium cromoglycate (Intal). *Acta Allergol* **22**, 487-9.

[19] Mesbah MK (1992) Determination of Khellin and Visnagin in Ammi visnaga fruits and in renal teas by HPLC. *Egypt J Pharm Sci* **33**, 897-904.

[20] Zhang T, Finn DF, Barlow JW, Walsh JJ (2016) Mast cell stabilizers. *Eur J Pharmacol* **778**, 158-168.

[21] Storms W, Kaliner MA (2005) Cromolyn sodium: Fitting an old friend into current asthma treatment. *J Asthma* **42**, 79-89.

[22] Rang HP, Dale MM (2003) Mechanism of Action 8. *Pharmacology*, Churchill Livingstone, Ed., Fifth Edition.

[23] Cox JSG (1977) *Pharmacological and Biochemical Properties of Drug Substances*, Goldberg ME, ed. American Pharmaceutical Association, Washington, D.C.

[24] Theoharides TC, Sieghart W, Greengard P, Douglas WW (1980) Antiallergic drug cromolyn may inhibit histamine secretion by regulating phosphorylation of a mast cell protein. *Science* **207**, 80-82.

[25] Foreman JC, Hallett MB, Mongar JL (1977) Site of action of the antiallergic drugs cromoglycate and doxantrazole. *Br J Pharmacol* **59**, 473-474.

[26] Oka T, Kalesnikoff J, Starkl P, Tsai M, Galli SJ (2012) Evidence questioning cromolyn's effectiveness and selectivity as a "mast cell stabilizer" in mice. *Lab Invest* **92**, 1472-1482.

[27] Wyss-Coray T, Rogers J (2012) Inflammation in Alzheimer disease-a brief review of the basic science and clinical literature. *Cold Spring Harb Perspect Med* **2**, a006346.

[28] Zhang C, Griciuc A, Hudry E, Wan Y, Quinti L, Ward J, Forte AM, Shen X, Ran C, David R. Elmaleh DR, Tanzi RE (2018) Cromolyn reduces levels of the Alzheimer's disease-associated amyloid β-protein by promoting microglial phagocytosis. *Sci Rep* **8**, 1-9.

[29] Granucci EJ, Griciuc A, Mueller KA, Mills AN, Le H, Dios AM, McGinty D, Pereira J, Elmaleh DR, Berry JD, Paganoni S, Cudkowicz ME, Tanzi RE, Sadri-Vakili G (2019) Cromolyn sodium delays disease onset and is neuroprotective in the $SOD1^{G93A}$ Mouse Model of amyotrophic lateral sclerosis. *Sci Rep* **9**, 17728.

[30] Bedor N, Zupan J, Selk S (1980) Improved delivery through biological membranes. VII. Dermal delivery of cromoglycic acid (cromolyn) via its prodrugs. *Int J Pharm* **7**, 63-75.

[31] Pajouhesh H, Lenzb GR (2005) Medicinal chemical properties of successful central nervous system drugs. *NeuroRX* **2**, 541-553.

[32] Using oral inhalation of micronized cromolyn, the average Cmax in CSF, indicative of drug delivery to the brain, was found to be 0.24±0.077 ng/ml. Elmaleh DR, Elmaleh, MD (2019) *Dispenser for dry-powder inhalation devices*. US20190321571 A1 2019-10-24.